CrystEngComm

Accepted Manuscript

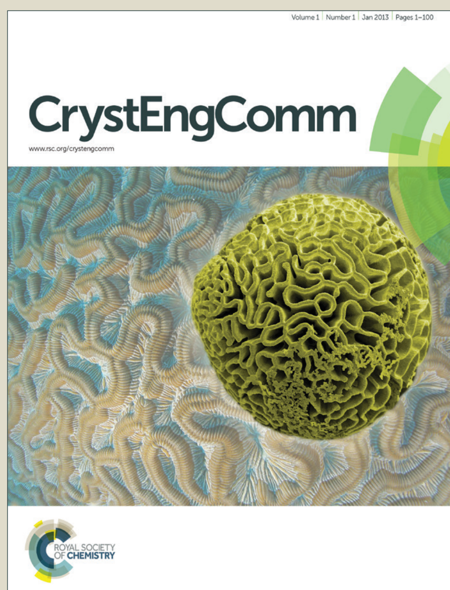

This is an *Accepted Manuscript*, which has been through the Royal Society of Chemistry peer review process and has been accepted for publication.

Accepted Manuscripts are published online shortly after acceptance, before technical editing, formatting and proof reading. Using this free service, authors can make their results available to the community, in citable form, before we publish the edited article. We will replace this *Accepted Manuscript* with the edited and formatted *Advance Article* as soon as it is available.

You can find more information about *Accepted Manuscripts* in the Information for Authors.

Please note that technical editing may introduce minor changes to the text and/or graphics, which may alter content. The journal's standard Terms & Conditions and the Ethical guidelines still apply. In no event shall the Royal Society of Chemistry be held responsible for any errors or omissions in this *Accepted Manuscript* or any consequences arising from the use of any information it contains.

ROYAL SOCIETY OF CHEMISTRY

www.rsc.org/crystengcomm

High Quality InP Nanopyramidal Frusta on Si

Wondwosen Metaferia[a] *Apurba Dev*[a], *Himanshu Kataria*[a], *Carl Junesand*[a], *Yan-Ting Sun*[a], *Srinivasan Anand*[a], *Juha Tommila*[b], *Galia Pozina*[c], *Lars Hultman*[c], *Mircea Guinb*[b], *Tapio Niemi*[b] *and Sebastian Lourdudoss*[a*]

[a] Laboratory of Semiconductor Materials, KTH, Electrum 229, 164 40 Kista, Sweden

[b] Optoelectronics Research Centre, Tampere University of Technology, FIN-33101 Tampere, Finland

[c] Thin Film Physics Division, Department of Physics (IFM), Linköping University, S-581 83 Linköping, Sweden

*corresponding author - slo@kth.se

Abstract: Nano size octagonal pyramidal frusta of indium phosphide are selectively grown from circular openings on silicon dioxide mask deposited on indium phosphide and indium phosphide pre-coated silicon substrates. The eight facets of the frusta are determined to be {111} and {110} truncated by a top (100) facet. The size of the top flat surface can be controlled by the diameter of the openings in the mask and separation between them. The limited height of the frusta is attributed to the kinetically controlled selective growth on the (100) top surface. Independent analyses with photoluminescence, cathodoluminescence and scanning spreading resistance measurements confirm certain doping enrichment in the frustum facets. This is understood to be due to the crystallographic orientation dependent dopant incorporation. The blue shift from the respective spectra is the result of this enrichment exhibiting Burstein-Moss effect. Very bright panchromatic cathodoluminescence

CrystEngComm Accepted Manuscript

images indicate that the top surfaces of the frusta are free from dislocations. The good optical and morphological quality of the nanopyramidal frusta indicates that the fabrication method is very attractive for the growth of site-, shape-, and number-controlled semiconductor quantum dot structures on silicon for nano photonic applications.

1. Introduction

The use of semiconductor quantum dot (QD) structures for optoelectronics[1,2] and photovoltics[3] is becoming more and more attractive. Due to a delta function like density of states and strong electron and hole confinement, QDs offer a low and temperature-insensitive threshold current density and large band width for lasing [4, 5]. Using QDs as single photon sources [6, 7, 8] is another novel application for quantum information processing [9] and quantum computing [10]. In the quest of light source for photonic integration on silicon substrate, QDs based on III-V semiconductor materials are shown to be suitable candidates[11, 12]. To this end, significant attention has been given to fabricate device quality III-V based quantum dots on III-V as well as Si wafers by various approaches. Among various approaches for device quality QD fabrication, the Stranski–Krastanov (SK) growth mode is a well-established method to fabricate high density QDs with good optical quality although the challenge to fabricate size-, shape-, and number- controlled quantum dots is still being addressed. To achieve single QD emission for advanced quantum functional devices such as nanolasers and single photon sources, precise position- and number control of a few down to a single QD is required [13]. This can be achieved by predefined nucleation site of a quantum dot via selective area growth epitaxy of host material prior to the growth of QDs. Selective area growth (SAG) of InP and GaAs truncated pyramidal structures on InP [14] and GaAs [15], respectively, were studied and control of number and position of InAs QDs on the top of the pyramids was achieved. In addition to providing high degree of freedom in control of site and density of the QDs, this approach also avoids unwanted nearby emitters since part of the sample other than

CrystEngComm Accepted Manuscript

the opening for selective area growth of the pyramids is covered by a dielectric mask which offers high degree of reproducibility. In addition, the pyramids help to separate the QDs from the initial substrate. The latter is advantageous to eliminate the high density of defects at the substrate/QD interface especially in case of heteroepitaxy of highly mismatched III-V based QDs on silicon. Besides, it is attractive to conduct QD growth of a III-V material on silicon provided with the same III-V seed layer to enable heteroepitaxial QD by SAG.

In this paper, we report SAG of high quality InP nano pyramidal frusta (NPF) from circular hole openings in silicon dioxide mask on InP and InP precoated Si substrates. The growth was conducted in a hydride vapor phase epitaxy (HVPE), a near-equilibrium process perfectly suitable for SAG. Scanning electron microscopy (SEM) and atomic force microscopy (AFM) are used to study the surface morphology and dimensions of the NPF. We show that size of the top flat surface of the NPF can be controlled by the diameter and center-to-center spacing of the circular hole openings in the oxide mask. In addition, the AFM study shows that the NPF is octahedral in shape and the top flat surface is (100) plane surrounded by eight low index planes of {111} and {110} planes. In order to use these templates for the growth of high quality quantum dot structures, their optical property is of fundamental importance especially in the case of hetreoepitaxy. The optical quality of the NPF was studied by room temperature cathodoluminescence (CL). We discuss the dislocation filtering mechanism in relation to the epitaxial necking effect and effect of reduced growth area. We also report and discuss the electrical properties of the NPF by scanning spreading resistance microscopy (SSRM) and compare with that of InP grown on unpatterned (planar InP) substrate.

2. Experimental

Two sets of samples from n-InP (100) misoriented 2° toward <110> substrate (called n-InP here after) and InP precoated Si (100) 4° off oriented toward <111> substrate (called InP(seed)/Si hereafter) were prepared. Plasma enhanced chemical vapour deposition

CrystEngComm Accepted Manuscript

(PECVD) was used to deposit 150 nm SiO_2 mask on the first set of samples and 90 nm SiO_2 mask on the second set of samples. Circular hole openings were made by soft ultraviolet nanoimprint lithography (UV-NIL) [16] in SiO_2 mask. The first set of samples contained two samples, n-InP and InP(seed)/Si, each with two pattern fields, A and B, of square arrays of circular hole openings of diameter (D) 300 nm. In pattern field A, the center to center spacing (S) was 500 nm, and in pattern field B, 1μm. The fill factor, i.e., the ratio of the total open area (the area of all the circular holes) to the total pattern field area in A and B was 0.28 and 0.07, respectively. The second set of samples also contained two samples, n-InP and InP(seed)/Si, similar to set 1 but with D=120 nm, S=180 nm and a fill factor of 0.19. SAG of sulphur doped InP, in the openings on both sets of samples was conducted in an Aixtron low pressure hydride vapor phase epitaxy (LP-HVPE) reactor [17]. The targeted sulphur concentration (electron concentration) in the grown InP was $5x10^{18}$ cm^{-3}, which is on the same order of magnitude as that in the n-InP substrate. The growth times were 2.5 minutes on the first set of samples and 15 minutes on the second set of samples. Growth temperature of 590 °C and V/III ratio of 10 (i.e., PH_3/InCl =10) were used in all cases. The reactor pressure was maintained at 20 mbar and the total gas flow was 900 sccm. Figure 1 shows schematics of circular hole openings in SiO_2 mask on InP(seed)/Si. The sample description and growth parameters are summarized in table 1. InP grown from the openings were characterized by, SEM, CL, AFM and SSRM. CL measurements were done using a MonoCL4 system integrated with a FEG cathode LEO 1550 Gemini SEM equipped with a CCD detector and a Peltier-cooled GaAs photomultiplier tube for data acquisition. AFM and SSRM measurements were done using a Digital Instrument's Nanoscope Dimension 3100 SPM system, equipped with an SSRM module. Commercial super sharp Si tip for the AFM taping mode morphological measurements and boron doped diamond coated silicon tips with force constants ~ 6 N/m (Nanosensors GmbH) for SSRM measurements were used.

CrystEngComm Accepted Manuscript

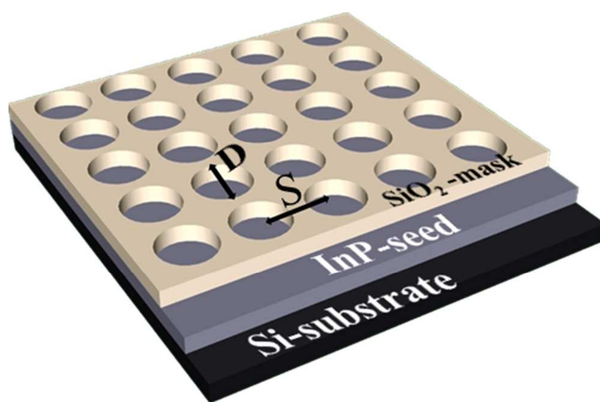

Figure 1: Schematics of nanoimprinted circular holes of diameter D and center to center spacing of S on InP(seed)/Si.

Table 1: Summary of samples and growth conditions

Sample sets	Substrate	Opening hole dimensions and Fill factor		Growth conditions
Set 1	n-InP	Field A D=300 nm, S=500 nm Fill factor =0.28	Field B D=300 nm, S=1000 nm Fill factor=0.07	Growth time =2.5 min Temp.=590 ^{0}C V/III=10
	InP(seed)/Si			
Set 2	n-InP	D=120 nm S=180 nm Fill factor 0.19		Growth time =15 min. Temp.=590 ^{0}C V/III=10
	InP(seed)/Si			

3. Results and Discussion

3.1. Morphological Studies

Figures 2(a) and 2(b) depict the SEM images of selectively grown n-InP nano pyramidal structures on the first set of samples with pattern field A on n-InP and InP(seed)/Si, respectively. The growth is highly selective without any nucleation on the mask surface. This is due to the equilibrium nature of hydride vapor phase epitaxy which allows for re-evaporation of the adsorbed InCl molecule on the dielectric mask [18]. It is found that the shape of the grown structure is a truncated pyramid, called pyramidal frustum, with eight sides

CrystEngComm Accepted Manuscript

regardless of the hole dimension and separation and substrate type. The side wall angle with respect to (100) top surface of the octagonal frustum was determined by AFM line scan of height image taken after removing the oxide mask and it was found to be 45° and 54° for the line scans made 45° to each other (along lines I and II in the inset of figure 2(c)), which indicates the corresponding side walls of the frustum are {110} and {111} planes, respectively. Figure 2(c) shows how the AFM line scan along line I is used to determine the side wall angle from the top flat surface of the NPF; the inset is the AFM height image of an NPF on InP(seed)/Si and the lines indicate the scan paths and figure 2(d) shows AFM amplitude image of an NPF on InP substrate with all facets labeled.

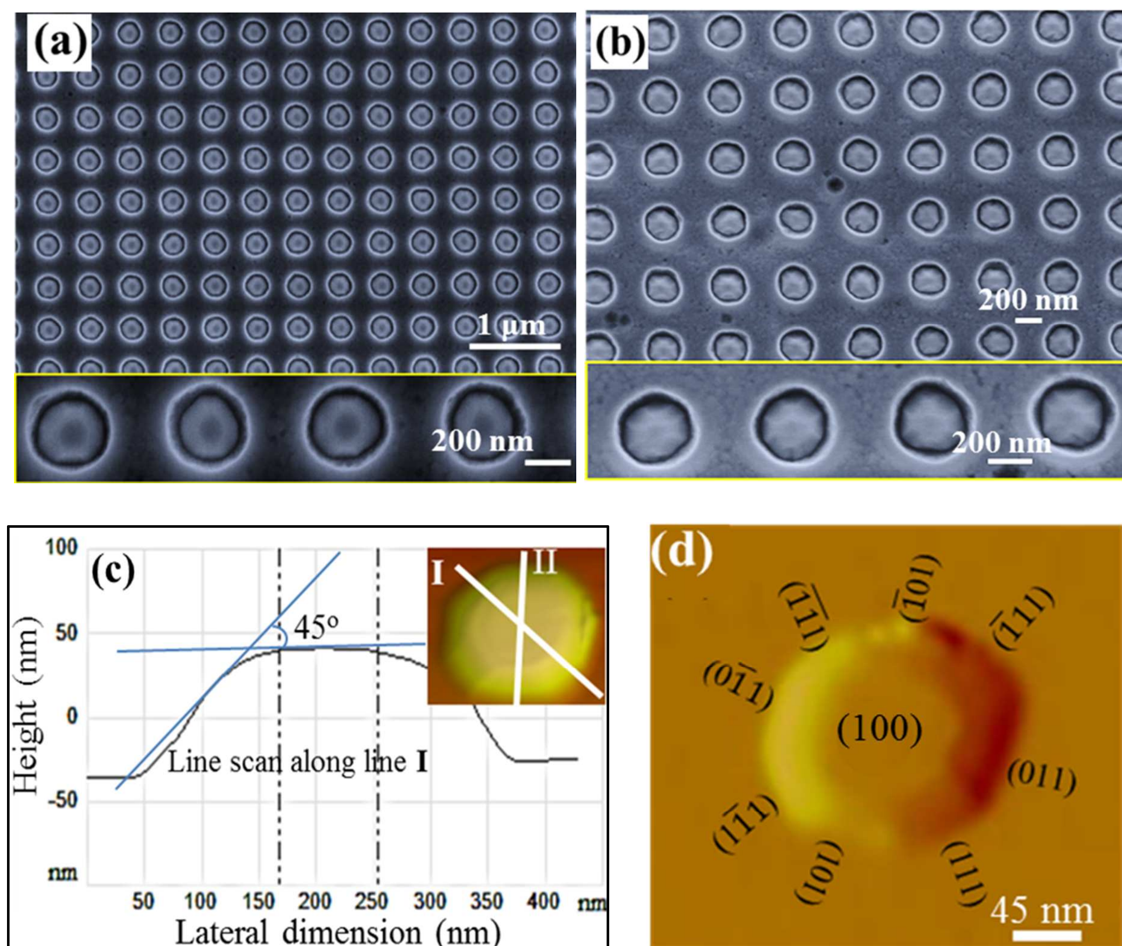

Figure 2. SEM image of InP naopyramidal frusta from sample set 1 with pattern field A grown on (a) n-InP and (b) on InP(seed)/Si; (c) AFM line scan of a frustum on InP(seed)/Si

CrystEngComm Accepted Manuscript

and the inset is the AFM height image showing the different facets and the scan path (I and II) and (d) AFM amplitude image of an NPF on InP substrate with all facets labeled.

As can be seen from the SEM images in figures 2(a) and 2(b) (lower panels) the symmetry of the truncated octahedral pyramids slightly varies. We observe that it is affected by the shape of the circular hole; a symmetric octagonal NPF is seen from a perfect circular hole.

Both sets of samples were characterized by AFM after the oxide mask was removed. In figure 3, we present the 3D AFM height image of NPF on the same set of samples whose SEM images are shown in figures 2(a) and 2(b).

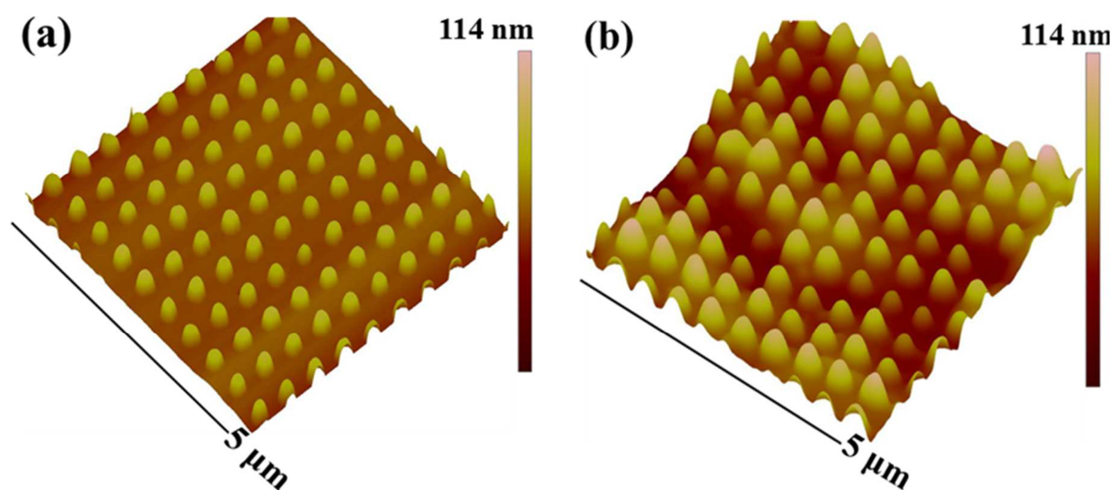

Figure 3. 3D 5x5 μm^2 surface rendering AFM images of NPF on; (a) n-InP and (b) InP(seed)/Si substrates of sample set 1 with pattern field A.

Whereas the NPF on n-InP substrate are homogeneous in size as seen in figure 3(a) those on InP (seed)/Si substrate vary in size (both vertical and lateral), see figure 3(b). This variation in size is understood to be due to the rough/uneven surface morphology/topography of the original seed layer, which has a root mean square (RMS) surface roughness of ~21 nm and a topographical variation of 50 nm (crest to trough) [19]. More importantly, the topography of the seed layer and hence the deposited oxide mask is uneven. The result is that at some regions, it is beyond the flexibility limit of the NIL stamp to get equal size openings on the dielectric

CrystEngComm Accepted Manuscript

mask. From figure 3 (b), it appears that the size of the NPF and the topographical variation of the InP seed layer can be correlated, i.e., the large NPF to the topographically elevated regions while smaller ones in the topographically lower regions. Thus, the size of the NPF is varying largely due to the uneven size of the imprinted openings. It has been shown that the morphology of InP(seed) layer can be further improved through chemical mechanical polishing [19], which however, was not employed in the current experiments.

Table 2 summarizes the dimensions of the NPF obtained from the AFM studies. The size of the top flat surface of the frusta is expressed in terms of distance between the opposite edges of the octagon, i.e., the diameter of the inner circle of the octagon. This was measured from the AFM line scans made perpendicular to each other. The difference between the two line scan measurements was insignificant. The average height was also measured from the AFM line scan from the substrate surface to the top of the frusta as shown in figure 2(c). The height and flat top surface diameter values presented in table 2 are the average values calculated from the measurements from several NPF.

Table 2: Dimensions of the NPF from both sets of samples

Sample		Fill Factor	Growth time (min)	Substrate	Average Height (nm)	Top Surface Diameter (nm)
Set 1	A	0.28 (D=300nm; S=500 nm)	2.5	n-InP	80±3	90±2
				InP(seed)/Si	79±12	91±7
	B	0.07 (D=300nm; S=1000nm)		n-InP	50±2	110±3
				InP(seed)/Si	49±4	111±5
Set 2		0.19 (D=120nm; S=180nm)	15	n-InP	41±3	30±2
				InP(seed)/Si	39±8	31±10

From table 2, it is evident that the results obtained from the openings on n-InP substrate and on InP(seed)/Si are very similar and hence the growth mechanisms may not be different for different substrates.

CrystEngComm Accepted Manuscript

Although the experiments were carried out only with three filling factors and two growth times, the following obtained results are helpful in gaining qualitative understanding of the underlying growth mechanisms of the NPFs: (i) The SEM and AFM images of figure 2 clearly show that the NPFs are contained within the opening area, i.e., there is no lateral growth resulting in mask encroachment. This absence of lateral growth is understood to be due to the formation of low index planes of slow growth rate (or stopping planes) already at the initial stages of growth. This indicates that once these stopping planes are formed, all the subsequent growth that takes place is predominantly vertical. (ii) The above argument suggests that the vertical growth can take place only with the supply of growth rendering species on the emerging (100) flat surface of the NPF whose area constantly shrinks with growth time. It also suggests that since the growth is contained within the opening, NPF from a smaller opening should result in shorter NPF with smaller flat surface. This is what is observed in Table 2, where sample from set 2 (with D=120 nm) results in NPFs of lower height and lower flat surface area with respect to the samples of set 1 (with D = 300 nm) although these two sets have different spacings. (iii) From the measurement of the heights of the NPF on both sets of samples, it is found that the vertical growth rate is in the range of 2 to 32 nm/minute. It is to be pointed out that this growth rate is approximately 1-2 orders of magnitude lower than what has been observed on the growth on (non-patterned) planar reference samples (200 nm/minute) conducted simultaneously with the two sets of samples. This observation might appear contradictory to what happens during SAG where the additional growth species adsorbed on the masked surface are transported to the open surface contributing to an enhanced growth rate compared to planar growth[20,21]. It has been shown in SAG conducted in MOVPE that for very small fill factors <10%, even though the supply of the growth species to the open area from the masked area is very high, the reaction kinetics on the (100) surface tends to limit the growth [22]. As the (100) surface area shrinks as the growth

CrystEngComm Accepted Manuscript

proceeds, as indicated above, this leads eventually to self-limiting growth (SLG). This mechanism which has also been invoked for the selective growth of GaN dots[23]. is found to be operative in our case also. Considering pattern field A and B of samples of set 1 with the same opening diameter and different spacings, NPF from B with larger spacing (lower fill factor) is shorter than that from A although both were grown for 2.5 min. If the SAG mechanism were operative, growth from B would have resulted in taller NPF (larger vertical growth rate) which is not the case. Hence the growth appears to be regulated by SLG mainly due to the kinetic limitation of growth on (100) surface. The larger flat surface of NPF from B than that from A is the result of the height difference of NPF from the opening of the same diameter, as the base of NPF is clamped within the opening. Extended growth time (15 min) of sample of set 2 resulting in lower height with respect to set 1 (2.5 min) can also be the result of this SLG mechanism although it can be the combined effect of smaller opening diameter.

In any case, our results indicate that by adjusting the growth time, the opening diameter and spacing, it is possible to achieve a desired size of top flat surface. Thus, by controlling the size of the top flat surface in such a way that it accommodates certain number of quantum dot structures, growth of number controlled semiconductor quantum dots at a controlled site is feasible [14, 24].

3.2. Cathodoluminescence Studies

The optical quality of the NPF was characterized by room-temperature panchromatic cathodoluminescence (PC-CL) with acceleration voltages of 5.5 keV. The SiO_2 mask was removed prior to the CL measurement. The PC-CL images along with the SEM images of the same area are shown in figures 4(a-d).

CrystEngComm Accepted Manuscript

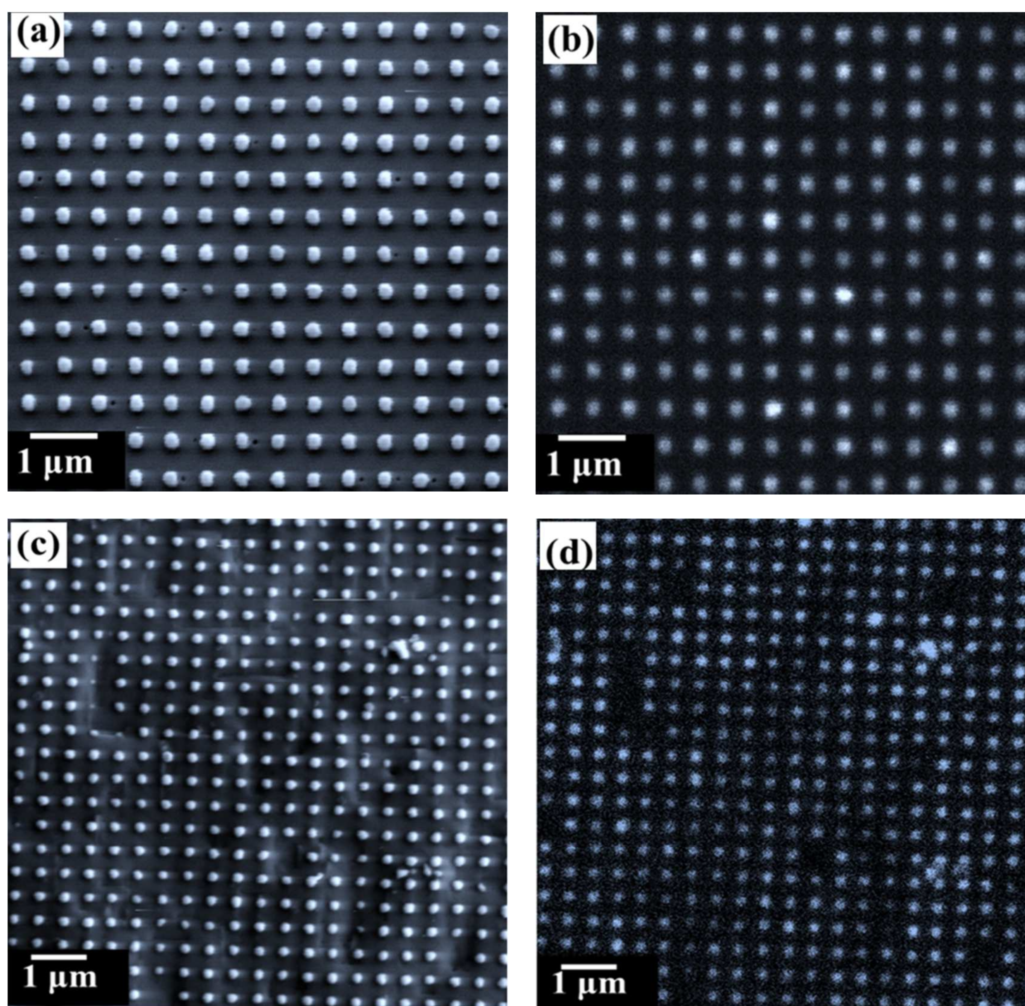

Figure 4. SEM and room temperature panchromatic CL images of InP NPF on (a): n-InP (SEM), (b): n-InP(PC-CL), (c): InP(seed)/Si(SEM) and (d): InP(seed)/Si(PC-CL) of sample set 1 with pattern field A, (the oxide mask was removed prior to the CL measurement).

Figures 4(a) and (c) show the SEM images and figure 4(b) and (d) are the corresponding PC-CL images taken from the NPF on n-InP and InP(seed)/Si substrates, respectively, of the first set of samples with pattern field A. Generally the PC-CL images of NPF from both substrates are very bright indicating the dominant radiative recombination of carriers, hence, structural defect-free or low-defect density NPF. Almost all of the NPF on n-InP substrate shown in figure 4(a) give bright CL contrast as shown in figure 4(b). From the SEM image in figure 4(c) we can see that there is a slight difference in the size of the NPF on InP(seed)/Si substrate

CrystEngComm Accepted Manuscript

confirming what was seen in the AFM image of figure 3(b); whereas large NPF yield bright CL image, the smaller ones resulted in a relatively weaker or no luminescence in the CL image (figure 4(d)). This is because for a constant CL excitation volume (excitation volume depends on the material atomic weight, atomic number and the acceleration voltage which is estimated to be <200 nm in this measurement condition), there will be more carriers in the InP (seed) excited for the smaller size NPF than the bigger ones where most of the exited carriers are from the NPF, hence brighter contrast. In the case of the NPF grown on InP(seed)/Si, the defect filtering mechanism involves epitaxial necking effect [25] where selective area growth and defect crystallography force the defects to the oxide side wall. In zinc blende cubic as in InP/Si system, misfit dislocations lie along <110> directions in the (100) growth plane while the threading segments rise up on (111) planes in <110> directions. Threading segments in <110> directions on the (111) plane make a 45° angle to the underlying Si (100) substrate. This effect results in the elimination of threading dislocations by terminating at the {111} planes of the NPF as shown in figure 5.

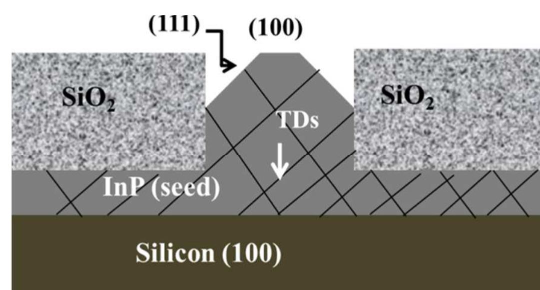

Figure 5. Schematic of cross section of an NPF on InP(seed)/Si (not to scale).

Note that the necking effect is more effective when aspect ratio, the mask thickness to the opening width is greater than 1. However, the effect of small growth area to reduce misfit and threading dislocations is more advantageous in this experiment. In a large area growth, growth starts from large surface that can contain higher density of fixed sources of dislocations (substrate dislocations and inhomogenities) [26]. In the InP(seed) layer on Si fixed sources of

CrystEngComm Accepted Manuscript

dislocations include threading dislocations (density 10^9 cm^{-2}) and surface roughness of about 21 nm (from a 25 μm x 25 μm AFM scan area) [19, 25]. During the growth of the epi-layer on large area, the numerous fixed sources of dislocations will propagate to the layer as well as produce dislocation interaction and multiplication events, further increase the dislocation densities [26]. On a small growth area as in this experiment, the number of fixed sources present which can relax the film is small, and the threading dislocations will move a smaller distance before reaching the mask sidewall. In addition termination of the dislocations at a free film edge is energetically favorable and the edge, the side facets in this case will therefore provide some pinning of the dislocations [28].

To study the quality of the NPF further, CL spectra were recorded from the individual NPF grown on both n-InP and InP(seed)/Si samples of set 1 with pattern field A and compared with the spectrum taken from the reference sample (n-InP grown on planar n-InP). Figure 6(a) compares the spectra (taken at the same measurement conditions) from a single NPF on n-InP and reference sample and figure 6(b) from, the NPF on InP(seed)/Si and planar InP(seed) layer on Si. Normalized spectra from the NPF on both InP(seed)/Si and on n-InP and the reference sample are given in figure 6(c). From figure 6(a) one observes that the CL intensity from the NPF on n-InP is slightly lower than the intensity from the reference sample, whereas from figure 6(b) the CL intensity from the NPF grown on InP(seed)/Si is about ten times stronger than that of the InP(seed) layer. We choose to assess the quality of the NPF on the two substrates with respect to the reference n-InP layer grown on planar n-InP substrate by comparing their full width at half maxima (FWHM) of their peaks. The spectra are recorded from several NPF on each substrate and no significant differences in the normalized intensity and FWHM of the emission line on the respective substrates are observed.

CrystEngComm Accepted Manuscript

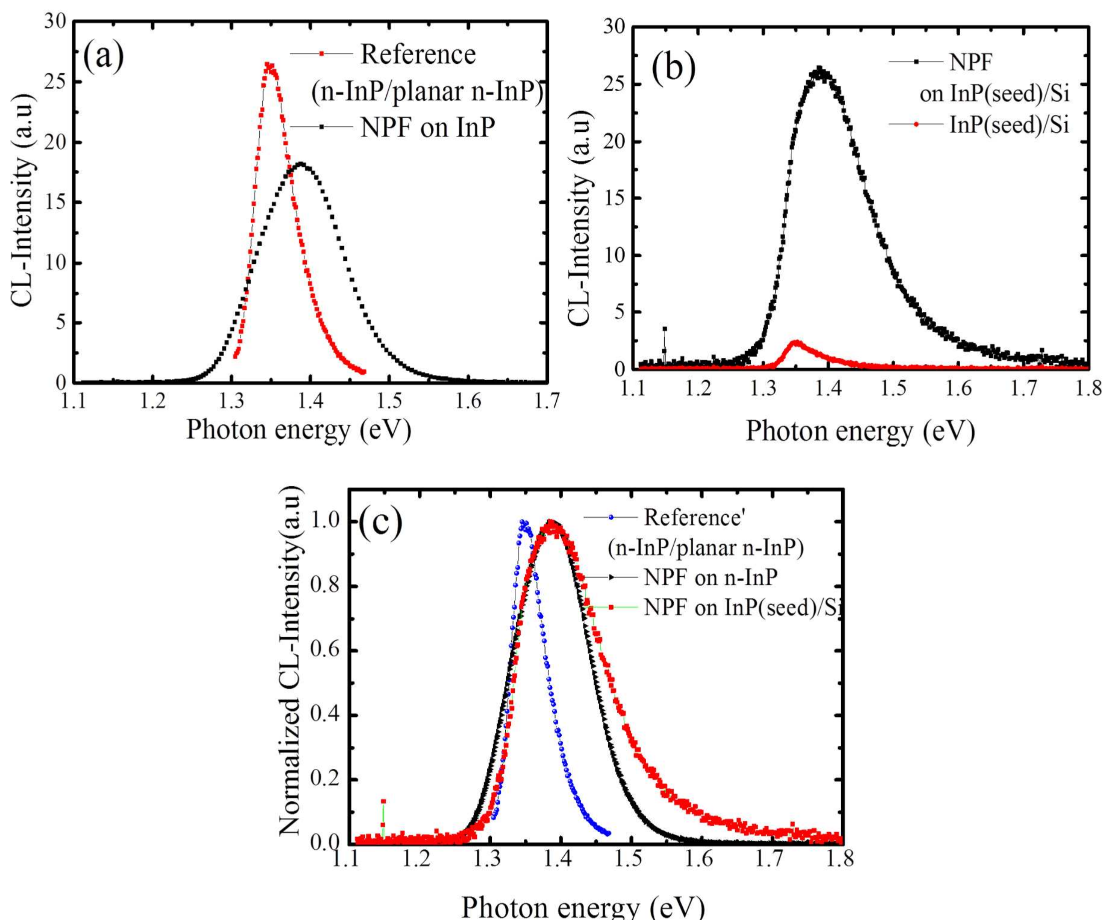

Figure 6. CL spectrum of a NPF on n-InP and InP(seed)/Si compared with the spectrum from the (a) reference sample, (b) InP(seed) layer, respectively, from sample set 1 of field A, and (c) normalized intensity spectra from the NPF in (a) and (b) and the reference sample.

As can be seen from figures 6(a-c), in all spectra taken from NPF on n-InP and InP(seed)/Si substrates, their FWHM is broader and blue shifted (~0.5 eV) compared to the reference sample. The FWHM of the spectra from NPF on n-InP and InP(seed)/Si substrates and the reference sample are 124 meV, 138 meV, and 68 meV, and their peak positions are 1.39, 1.39 and 1.35 eV, respectively. The difference in FWHM between the NPF and the reference layer is understood to be due to the doping effect. According to a study by Bugajski and Lewandowski in reference [29], for highly doped (above the degeneracy limit, i.e, ~$5x10^{17}$ cm^{-3}) n-InP, about one order of magnitude increase in doping level causes approximately two-fold

CrystEngComm Accepted Manuscript

photoluminescence (PL) line broadening, which is the broadening observed in our CL measurements of the NPF compared to the reference sample. In a supplementary experiment on n-InP substrate, we observed that without any change in the peak position, the line-width from CL to be 68 meV, which is broader than that of the PL spectra, which is 55 meV. A similar trend also has been observed by Roderiguez et al in [30]. Hence, the line broadening in CL spectrum can be explained in the same way as that of PL. From the photoluminescence study of n type InP at room temperature, the relation between doping level and the difference in band gap energy is [29]:

$$\Delta E_g(n) = 22.5 \times 10^{-9} n^{1/3} (eV), \qquad (1)$$

where $\Delta E_g(n)$ is the change in the band gap energy caused by a doping concentration of n in cm^{-3}. By using this relation, we found doping concentration of 5.6 $x10^{18} cm^{-3}$ for the change in the band gap energy of 40 meV, which is observed in the CL spectra of the NPF on both kinds of substrates. This doping concentration is higher than what has been used to dope the NPF during growth, which is ~5 $x10^{18}$ cm^{-3}. In the same study by Bugajski and Lewandowski in [29], doping concentration of n in cm^{-3}, resulting in spectral broadening of $\Delta E(n)$ in eV can be determined with a 10 % uncertainty as in equation (2).

$$\Delta E(n) = 2.22 \times 10^{-14} n^{1/3} (eV). \qquad (2)$$

We found a spectral width of 70 meV from equation (2) caused by a doping concentration of 5.6 $x10^{18}$ cm^{-3} obtained from equation (1). This value is about half of the experimental value. However, as we discussed previously, there is a difference in CL and PL line-width and we believe that the values would be close to each other if the exact difference of the line-width in the CL and PL for the NPF on both substrates is known. The yet unanswered question is therefore, why the doping level in the NPF is higher than that of the reference sample which

CrystEngComm Accepted Manuscript

was meant to be doped with the same doping concentration as the NPF and hence causes the broadening of the CL spectra. One possible explanation is the enhanced doping concentration in the side facets of the frusta due to crystallographic dependent dopant incorporation as observed by Y.T. Sun et al[31]. To verify if this is the case in this experiment, we conducted a SSRM studies on NPF grown on n-InP substrate and the reference sample. The SSRM studies and results are presented in the following section.

3.3. SSRM studies

In SSRM technique, the local resistance of the near surface region of the sample is obtained by measuring the electrical current flowing between a conductive-tip and the sample that is biased relative to the tip. A two-dimensional map of the resistance is obtained by scanning the probe over the sample surface. To achieve highest possible resolution the scanning was conducted at low applied forces maintaining a stable electrical contact. Figure 7(a) shows the SSRM current image of a representative NPF array on n-InP substrate of sample set1 with pattern field A measured at -1 V sample bias under ambient condition. The NPF are clearly visible, appearing bright in (current) contrast due to lower resistance compared to the substrate.

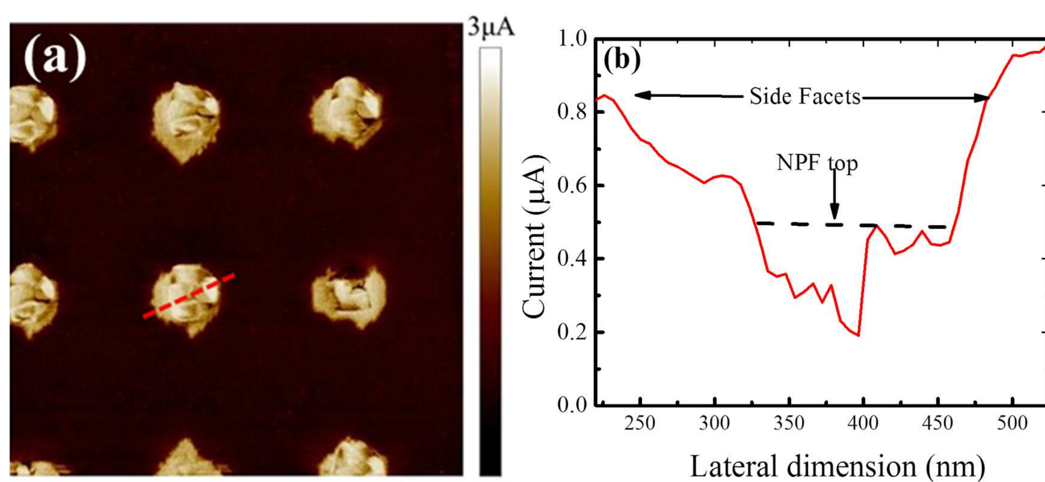

CrystEngComm Accepted Manuscript

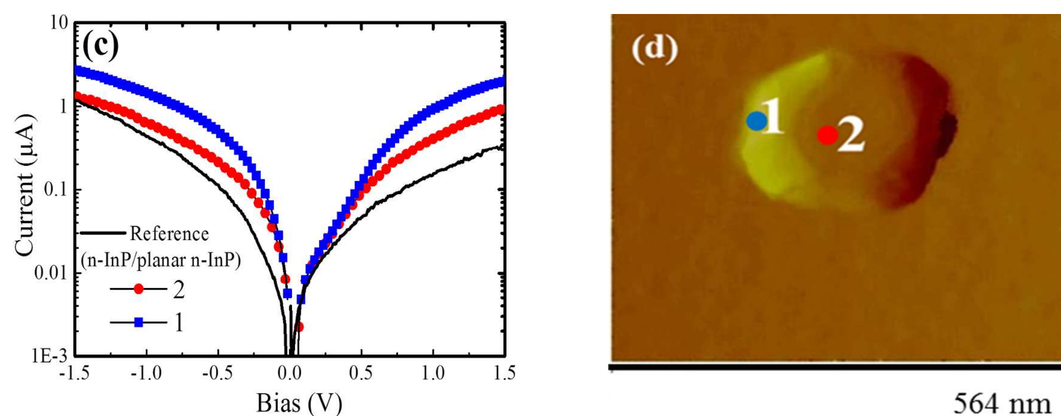

Figure 7. (a) SSRM current image of NPF array on n-InP substrate measured at -1V sample bias under ambient condition, (b) section analysis of the current in the NPF along the dotted line in (a), the current variation at different faces of the NPF indicated in the AFM image in (d), (c) the local I-V characteristics on the NPF and the reference sample (n-InP/planar n-InP) and (d) tapping mode AFM image showing the positions of 1 and 2 in (c) on the NPF.

Section analysis (along the red dotted line in figure 7(a)) presented in figure 7(b), exhibits 2-3 times higher current through the side surfaces than through the top surface. Several single nanopyramids investigated in different parts of the sample consistently reveal similar trend of higher conductivity at the side surfaces (facets) compared to the central top region. However, as seen from figure 7(a) the individual nanopyramids show distinct contrast variations suggesting local variations in the conductivity. This is also visible in the section data shown in figure 7(b), where the current spatially varies by as much as 0.3 μA in the region indicated as NPF top. Considering the reported SSRM lateral resolution of less than 10 nm for probes similar to ones used here[32], the observations strongly argue for the presence of local conductivity variations in the NPF. However, even a qualitative interpretation of the observed local current variations requires a full understanding of doping incorporation in these complicated NPF structures, and is not attempted here. In the above context, the SSRM

CrystEngComm Accepted Manuscript

measurements are used only for qualitative comparison of the conductivity of the NPF side-wall and top regions.

In separate measurements, using SSRM Local I-V (figure 7(c)) characteristics of a NPF were also measured. The measurements were made at the top central region of the NPF and at the side facets, approximately, in the vicinity of the blue and red dots indicated by numbers 1 and 2 in the tapping mode AFM topography image shown in figure 7(d). For comparison, the measured I-V characteristics of the reference InP layer grown at the same time as the NPFs is also presented in figure 7(c). The measured I-V characteristics are non-linear (figure 7(c)) indicating a Schottky-like contact and is consistent with earlier reports on SSRM measurements of InP [33]. However, the I-V characteristics of the reference InP layer shows a stronger rectifying behavior, while those of the NPF show symmetric behavior. The latter can be attributed to tunneling-dominated conduction indicating higher doping levels in the NPFs compared to the InP reference layer. Within the NPF the higher conductivity of the side facets reveals additional dopant incorporation in these facets (planes), and is consistent with previous observations [31]. Though it is not possible to deduce the exact dopant concentration difference between the reference layer and the NPF and compare the expected dopant difference that causes the CL broadening, we believe that the line shift and broadening are mainly due to Burstein–Moss effect caused by the filling of states close to the conduction band by the higher doping in the NPF. Thus, the measured band gap determined from the onset of interband absorption moves to higher energy, blue shifted.

CrystEngComm Accepted Manuscript

4. Conclusions

Selective area growth of InP nanopyramidal frusta on n-InP and Si substrates is reported. Well defined octagonal pyramidal frustum with (100) top surface surrounded by {111} and {110} facet planes are fabricated. Uniform size NPF on silicon can be produced by polishing the InP (seed) layer on Si. The size of the top flat surface of the NPF are controlled by the hole opening diameter and center-to-center spacing of the hole openings in the dielectric mask. The growth rate of the NPF is so low compared to the planar growth rate. This is due to the formation of growth stopping low index facet planes quickly that leads to reduce or stop the growth already at the initial stage of growth and so that no growth occurs afterwards. This can help to have good control of the size of NPF and make the process reproducible. As confirmed by the panchromatic cathodoluminesence measurement the NPF is of high optical quality even on InP(seed)/Si substrate and showed the effective defect filtering. The spreading resistance microscopy measurement revealed that the NPF are highly doped compared to the n-InP grown on planar n-InP substrate, reference sample, indicating enhanced crystallographic orientation dependent dopant incorporation. The fact that the side facets appear brighter in current image from the SSRM study compared to the top flat (100) surface indicates that these facets are preferentially doped more. Therefore, the total doping density in the nanopyramidal frusta is higher than the planar surface on the reference sample. Hence, blue shift and broader cathodoluminescence spectrum from the NPF is attributed to the Burstein–Moss effect caused by the higher doping level. The controlled dimension, high optical and electrical qualities of the NPF are suitable for site and number controlled growth of semiconductor quantum dots for future silicon and nanophotonic applications

CrystEngComm Accepted Manuscript

Acknowledgments

The authors would like to acknowledge the financial support of Swedish Research Council through ADOPT Linné Center of Excellence and Intel Corporation. The Knut and Alice Wallenberg Foundation supported the Myfab network at KTH and the Ultra Electron Microscopy Laboratory at Linköping operated by the Thin Film Physics Division.

CrystEngComm Accepted Manuscript

References

1. H. Sakaki, in *Electron Devices Meeting, 2007. IEDM 2007. IEEE International*, 2007, pp. 9–16.
2. S. Fafard, K. Hinzer, and C. N. Allen, *Braz. J. Phys.*, 2004, **34**, 550–554.
3. P. V. Kamat, *J. Phys. Chem. Lett.*, 2013, **4**, 908–918.
4. Y. Arakawa and H. Sakaki, *Appl. Phys. Lett.*, 1982, **40**, 939–941.
5. M. Asada, Y. Miyamoto, and Y. Suematsu, *IEEE J. Quantum Electron.*, 1986, **22**, 1915–1921.
6. P. Michler, A. Kiraz, C. Becher, W. V. Schoenfeld, P. M. Petroff, L. Zhang, E. Hu, and A. Imamoglu, *Science*, 2000, **290**, 2282–2285.
7. E. Stock, T. Warming, I. Ostapenko, S. Rodt, A. Schliwa, J. A. To□fflinger, A. Lochmann, A. I. Toropov, S. A. Moshchenko, D. V. Dmitriev, V. A. Haisler, and D. Bimberg, *Appl. Phys. Lett.*, 2010, **96**, 093112.
8. K. Rivoire, S. Buckley, A. Majumdar, H. Kim, P. Petroff, and J. Vučković, *Appl. Phys. Lett.*, 2011, **98**, 083105–083105–3.
9. M. Förtsch, J. U. Fürst, C. Wittmann, D. Strekalov, A. Aiello, M. V. Chekhova, C. Silberhorn, G. Leuchs, and C. Marquardt, *Nat. Commun.*, 2013, **4**, 1818.
10. Y.-M. He, Y. He, Y.-J. Wei, D. Wu, M. Atatüre, C. Schneider, S. Höfling, M. Kamp, C.-Y. Lu, and J.-W. Pan, *Nat. Nanotechnol.*, 2013, **8**, 213–217.
11. T. Tatsumi, K. Tanabe, K. Watanabe, S. Iwamoto, and Y. Arakawa, *J. Appl. Phys.*, 2012, **112**, 033107–033107–5.
12. K. Tanabe, K. Watanabe, and Y. Arakawa, *Sci. Rep.*, 2012, **2**.
13. H. Wang, J. Yuan, T. Rieger, P. J. van Veldhoven, P. Nouwens, T. J. Eijkemans, T. de Vries, B. Smalbrugge, E. J. Geluk, and R. Nötzel, *Appl. Phys. Lett.*, 2009, **94**, 143103.
14. P. J. Poole, D. Dalacu, J. Lefebvre, and R. L. Williams, *Nanotechnology*, 2010, **21**, 295302.

CrystEngComm Accepted Manuscript

15. C.-K. Hahn, J. Motohisa, and T. Fukui, *Appl. Phys. Lett.*, 2000, **76**, 3947–3949.
16. A. Tukiainen, J. Viheriälä, T. Niemi, T. Rytkönen, J. Kontio, and M. Pessa, *Microelectron J*, 2006, **37**, 1477–1480.
17. S. Lourdudoss and O. Kjebon, *Sel. Top. Quantum Electron. IEEE J. Of*, 1997, **3**, 749 –767.
18. S. Lourdudoss, E. R. Messmer, D. Soderstrom, and O. Kjebon, in *1998 International Conference on Indium Phosphide and Related Materials*, 1998, pp. 785 –788.
19. C. Junesand, C. Hu, Z. Wang, W. Metaferia, P. Dagur, G. Pozina, L. Hultman, and S. Lourdudoss, *J. Electron. Mater.*, 2012, **41**, 2345–2349.
20. Y. D. Galeuchet, P. Roentgen, and V. Graf, *Appl. Phys. Lett.*, 1988, **53**, 2638–2640.
21. F. Olsson, M. Xie, S. Lourdudoss, I. Prieto, and P. A. Postigo, *J. Appl. Phys.*, 2008, **104**, 093112–093112–6.
22. Y. D. Galeuchet, P. Roentgen, and V. Graf, *J. Appl. Phys.*, 1990, **68**, 560–568.
23. C. Liu, P. A. Shields, Q. Chen, D. W. E. Allsopp, W. N. Wang, C. R. Bowen, T.-L. Phan, and D. Cherns, *Phys. Status Solidi C*, 2010, **7**, 32–35.
24. T. Tran, A. Muller, C. K. Shih, P. S. Wong, G. Balakrishnan, N. Nuntawong, J. Tatebayashi, and D. L. Huffaker, *Appl. Phys. Lett.*, 2007, **91**, 133104.
25. T. A. Langdo, C. W. Leitz, M. T. Currie, E. A. Fitzgerald, A. Lochtefeld, and D. A. Antoniadis, *Appl. Phys. Lett.*, 2000, **76**, 3700–3702.
26. E. A. Fitzgerald, in *Proceedings of the 16th Annual Conference on The Physics And Chemistry of Semiconductor Interfaces*, Avs, 1989, Vol. 7, Pp. 782–788.
27. W. Metaferia, C. Junesand, M.-H. Gau, I. Lo, G. Pozina, L. Hultman, and S. Lourdudoss, *J. Cryst. Growth*, 2011, **332**, 27–33.
28. J. Knall, L. T. Romano, D. K. Biegelsen, R. D. Bringans, H. C. Chui, J. S. Harris, D. W. Treat, and D. P. Bour, *J. Appl. Phys.*, 1994, **76**, 2697–2702.
29. M. Bugajski and W. Lewandowski, *J. Appl. Phys.*, 1985, **57**, 521–530.

CrystEngComm Accepted Manuscript

30. J. Rodriguez-Viejo, K. F. Jensen, H. Mattoussi, J. Michel, B. O. Dabbousi, and M. G. Bawendi, *Appl. Phys. Lett.*, 1997, **70**, 2132–2134.

31. Y. T. Sun, S. Anand, and S. Lourdudoss, *J. Cryst. Growth*, 2002, **237–239, Part 2**, 1418–1422.

32. O. Douheret, S. Bonsels, and S. Anand, *J. Vac. Sci. Technol. B Microelectron. Nanometer Struct.*, 2005, **23**, 61–65.

33. D. Ban, E. H. Sargent, S. J. Dixon-Warren, T. Grevatt, G. Knight, G. Pakulski, A. J. SpringThorpe, R. Streater, and J. K. White, *J. Vac. Sci. Technol. B Microelectron. Nanometer Struct.*, 2002, **20**, 2126–2132.

CrystEngComm Accepted Manuscript

Table of Contents Entry

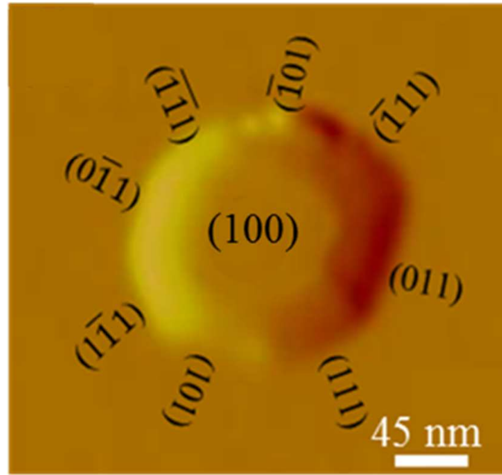

Octagonal nanopyramidal InP frusta grown selectively on silicon

CrystEngComm Accepted Manuscript